

# Coalescence of immersed droplets on a substrate

Dennis Hessling · Jacco H. Snoeijer · Jens Harting

the date of receipt and acceptance should be inserted later

**Abstract** The dynamics of droplets on substrates has a strong impact on microfluidic systems ranging from commercially available lab-on-chip systems to state of the art developments in open microfluidics. Coalescence of micro and nano droplets on a substrate has been studied extensively, but in previous studies the focus has been on the interface movement. Here, we use computer simulations to investigate coalescence of droplets immersed in another liquid, in an inertia-dominated regime and also investigate the droplet's internal flow field. It is found that qualitatively the dynamics is similar to coalescence in air, with the same self-similar growth laws. We here point out the ambiguity in the scaling argument for droplets of  $90^\circ$ , that shows itself in the velocities. We show that droplets with a contact angle below  $90^\circ$  exhibit a self-similar velocity field, and the corresponding scaling laws are identified. For drops of  $90^\circ$ , however, it is shown that the velocity field has a

more intricate structure that is beyond the usual scaling arguments invoked for coalescence.

**PACS** 47.55.df, 47.55.D-, 47.85.mb

## 1 Introduction

Commercially available microfluidic devices generally consist of closed channels. These are of advantage in order to prevent evaporation and allow to pump fluids by applying a pressure difference between inflow and outflow boundaries. However, keeping the channels clean is a serious problem due to clogging. Open microfluidic systems are an alternative route, where droplets and rivulets are confined to chemically patterned substrates containing wetting surface domains on a less wetting substrate [1,2,3,4,5,6]. While flow in chemical channels cannot be induced by pressure differences, capillary forces due to wettability gradients [7], or electrowetting [8] are a possible alternative. Another practical possibility are shear forces induced by a covering immiscible fluid [9]. The advantage of this approach is also that it prevents evaporation and contamination, e.g. with dirt or dust. In microfluidic systems and in open systems in particular, the separation and coalescence of micro and nano droplets is a common phenomenon. However, it occurs not just in microfluidics, but in various situations, such as cloud formation, film formation [10] or inkjet printing [11,12,13]. While sessile droplets with a contact angle of  $90^\circ$  are comparable to freely suspended droplets, sessile droplets of different contact angles are omnipresent and can have a significantly altered behaviour, as we show in this work. Many different phenomena are found in this process, like jumping of the coalescing droplets [14], a transition from coalescence to noncoalescence [15,11], variations in the meniscus

Dennis Hessling  
Materials innovations institute (M2i), Electronicaweg 25, 2628 XG Delft, Netherlands  
Department of Applied Physics, Eindhoven University of Technology, Postbus 513, 5600 MB Eindhoven, The Netherlands

Jacco H. Snoeijer  
Department of Applied Physics, Eindhoven University of Technology, Postbus 513, 5600 MB Eindhoven, The Netherlands  
Faculty of Science and Technology, University of Twente, Drienerlolaan 5, 7522 NB Enschede, The Netherlands

Jens Harting  
Forschungszentrum Jülich GmbH, Helmholtz Institute Erlangen-Nürnberg for Renewable Energy (IEK-11), Fürther Straße 248, 90429 Nürnberg, Germany E-mail: j.harting@fz-juelich.de  
Department of Applied Physics, Eindhoven University of Technology, Postbus 513, 5600 MB Eindhoven, The Netherlands  
Faculty of Science and Technology, University of Twente, Drienerlolaan 5, 7522 NB Enschede, The Netherlands

shape [16] and resulting behavior [17], mixing [18,19] or the growth rate dependence of the meniscus on the contact angle [20,21]. Furthermore, a large interest in droplets and bubbles submerged in a liquid exists [22, 23, 24, 25]. Often experiments on droplets are performed submerged [26], in order to reduce the influence of gravity, to scale diffusion [27, 28] or in order to study altered friction behavior [29, 30].

Of particular interest is the initial coalescence dynamics, just after the drops are brought into contact. The two drops become connected by a small liquid bridge that rapidly grows in time (Fig. 1). This rapid motion is due to the large curvature that induces a very large (negative) Laplace pressure, driving the liquid into the bridge between the two drops. This process has for example been studied extensively for freely suspended drops [31, 32, 33, 34, 35, 36]. Here we concentrate on drops on a substrate, which further complicates the geometry of the coalescence process [37, 38, 39, 17, 40, 20, 41]. An important observation is that the dominant direction of the flow is oriented from the center of the drops towards the bridge, such that the relevant scaling laws can be inferred from quasi-two-dimensional arguments [37, 38, 17, 40, 20]. Interestingly, for inertia-dominated coalescence it was shown that droplets of a  $90^\circ$  contact angle behave differently from those of a lower contact angle. Even small deviations from  $90^\circ$  lead to a faster growth of the bridge height in time, which can be described in terms of scaling laws. In particular, the inertial coalescence changes from  $t^{\frac{1}{2}}$  for  $90^\circ$ , to a  $t^{\frac{2}{3}}$  power law for smaller angles [40, 20]. In both cases the shape of the liquid bridge exhibits a self-similar dynamics, but with different horizontal and vertical scales when the contact angle reaches  $90^\circ$ .

In this paper we focus on the coalescence of sessile drops immersed in another liquid, as it is relevant in open microfluidics. This has been addressed in the viscous regime [41], for which both the drops and the surrounding fluid were highly viscous. Here we perform lattice Boltzmann simulations in the inertial regime and define the outer fluid to be of the same density as the coalescing droplets. We investigate how the bridge dynamics changes as a function of the contact angle and, to the best of our knowledge, for the first time investigate whether self-similar behavior can be identified in the velocity field. A detailed comparison to experiments [40] of drops in air is provided, pointing out similarities and differences with respect to immersed droplets. The paper starts with a description of the lattice Boltzmann method, and we pay particular attention to the initiation of the coalescence (Sec. 2). The central results are presented in Sec. 3 and the paper closes with a discussion in Sec. 4.

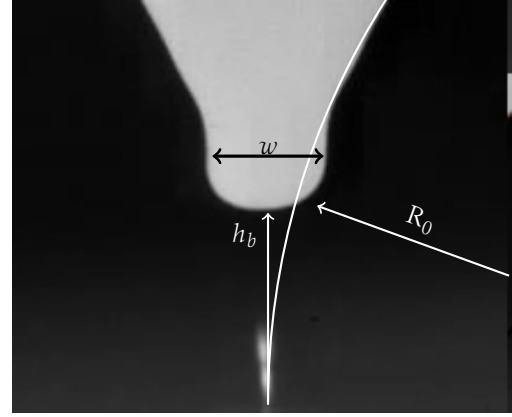


**Fig. 1** Snapshot of the bridge shape during coalescence from the experiment by Eddi et al. [40]. In this example the droplets have a contact angle of  $90^\circ$ . The bridge height  $h_b$ , initial droplet radius  $r_0$  and the horizontal scale  $w$  are marked in the image.

## 2 Simulation Method

### 2.1 The lattice Boltzmann method

The coalescence of droplets is a quasi 2D problem [37, 17, 40], so in favor of numerical speed we choose to perform our simulations in 2D. To investigate the coalescence of droplets on a substrate [1], we use the lattice Boltzmann method (LBM) [29, 42, 43] in a D2Q9 configuration [44, 45], that can be described by

$$f_i^\alpha(\mathbf{x} + \mathbf{c}_i \Delta t, t + \Delta t) - f_i^\alpha(\mathbf{x}, t) = -\frac{1}{\tau^\alpha} \left( f_i^\alpha(\mathbf{x}, t) - f_{ieq}^\alpha(\mathbf{x}, t) \right), \quad (1)$$

where  $f_i^\alpha(\mathbf{x}, t)$  is a probability distribution function of particles with mass  $m$  of component  $\alpha$  at position  $\mathbf{x}$  and time  $t$ , following the discretized velocity direction  $\mathbf{c}_i$ . The left hand side of (1) is the streaming step, where the probability distribution functions of the fluid  $\alpha$  is distributed to the surrounding lattice sites. The timestep  $\Delta t$ , the lattice constant  $\Delta x$  and the mass  $m$  of this process are chosen unity for simplicity. On the right hand side of (1), the collision step, these distributions relax towards an equilibrium distribution

$$f_{ieq}^\alpha(\mathbf{x}, t) = w_i \rho^\alpha \left[ 1 + \frac{\mathbf{c}_i \cdot \mathbf{u}}{c_s^2} + \frac{(\mathbf{c}_i \cdot \mathbf{u})^2}{c_s^2} - \frac{(L B u^\alpha)^2}{2 c_s^2} \right] \quad (2)$$

on a timescale determined by the relaxation time  $\tau$ . The relaxation time is directly proportional to the kinematic viscosity as  $\nu^\alpha = \frac{2\tau^\alpha - 1}{6}$ . For simplicity  $\tau^\alpha$  is chosen unity here. Forces can be added by shifting the equilibrium distribution function and thereby implicitly adding

an acceleration [46]. Multiple components may coexist on every lattice site. Via forces, these can interact with each other. Here we follow the method described by Shan and Chen [46]

$$\mathbf{F}^\alpha(\mathbf{x}, t) = -\rho^\alpha(\mathbf{x}, t)g^{\alpha\bar{\alpha}} \sum_{i=1}^9 \rho^{\bar{\alpha}}(\mathbf{x} + \mathbf{c}_i, t)\mathbf{c}_i. \quad (3)$$

These interaction forces cause the separation of fluids and a surface-tension  $\gamma$ . Here we restrict ourselves to two fluids and refer to them as “red” and “blue” fluids. The width of fluid interfaces and the resulting surface tension are governed by the interaction strength parameter  $g^{\alpha\bar{\alpha}}$ , which is chosen as 0.9 for all shown simulations. This results in a surface tension of  $\gamma = 1.18 \frac{\Delta x m}{\Delta t^2}$ . Our choice of parameters implies that the viscous length scale  $\frac{\rho^\alpha \nu^{\alpha^2}}{\gamma}$  is comparable to the lattice unit  $\Delta x$ . The resulting scale for the coalescence is thus much larger than the viscous length, ensuring we are in the inertial regime of coalescence [33, 31, 40].

In this setup the droplets sit on a horizontal flat substrate. The horizontal no slip boundary sites  $w$  defining the substrate are modified to include a pseudo-density [30] equal to the average of the surrounding fluid sites. Interactions as described in (3), with interaction parameters  $g^{\alpha w}$  and  $g^{\bar{\alpha} w}$  cause a contact angle [47, 30]. In equation (3)  $g^{\alpha w}$  and  $g^{\bar{\alpha} w}$  act in place of the interaction strength parameter and scale the absolute interaction force of the wall on the fluids, but  $g^{\alpha w} - g^{\bar{\alpha} w}$  defines the contact angle [47]. The parameters are chosen as  $g^{\alpha w} = -g^{\bar{\alpha} w}$  to minimize absolute forces.

Using full slip boundaries to effectively mirror the system at the symmetry axis, the computational domain and therefore computational cost is halved. The computational costs have to be considered for the two following reasons: as we are interested in obtaining the meniscus height over time with sufficient accuracy, we need to scale our entire system to a large resolution. A second numerical effect to consider is that, because of the finite width of the interface, the interface and the resulting fluid behavior can be overrepresented. To avoid this, the interface thickness should be small, as compared to the droplet radius [21]. The droplet radius at a contact angle of  $90^\circ$  is chosen to be  $900\Delta x$ , so that the interface thickness results in about 0.5 % of the droplet radius. It was found empirically that this drop size is sufficient to achieve reproducible results for the resulting hydrodynamics. All fluid volumes and system dimensions are kept constant and only the wall interaction parameters  $g^{\alpha w} = -g^{\bar{\alpha} w}$  and a horizontal shift length, that brings the droplets into contact, are adjusted for all subsequent simulations of decreasing contact angles.

## 2.2 Initialization of coalescence

Both in experiment and in simulations, it is challenging to initiate coalescence and to define the time  $t = 0$  that marks the start of the coalescence. Here we provide technical details on how the simulations were performed. A first problem is that the width of the diffuse interface and the fluid pressures are dependent on the  $g^{\alpha\bar{\alpha}}$  fluid parameters, so that it is not possible to predict beforehand the correct densities at all positions. This is why equilibration during initialization is required. A lack of correct initialization will lead to strong artefacts, such as an enclosed bubble for droplets of a  $90^\circ$  contact angle that can be avoided with careful initialization. To do so, we first equilibrate a horizontally centered single droplet at the wetting wall before a second drop is introduced. The introduction of a second drop, and the initiation of coalescence is a subtle matter by itself. Here we shift the droplet to a system boundary with a full slip boundary condition. This effectively mirrors the droplet, as is depicted in the schematic figure 2(a). This is a magnified section of the system at the meniscus after shifting the droplet. Here, the effectively mirrored part is shown in slightly opaque and density profiles at different cross sections of the diffuse interface are sketched in Figs. 2(b) and 2(c). The mirrored part of the system shown in Fig. 2(a) does not need to be simulated, which reduces the simulation time. The density gradients shown in Fig. 2(b) of the two fluids exemplary show a transition from a majority of one fluid to the other, as for instance in the 1D cross section in Fig. 2(a), marked with “Diffuse Interface”. This schematic representation of a diffuse interface identifies that the position of an according sharp interface is not clearly defined. Accordingly, the shift to the full slip boundary can be executed in different ways, like shown in Fig. 2(c). Here the schematic red density gradient stays in place, while the density gradient of the other droplet is shifted. The second gradient is drawn multiple times, transitioning from left to right.

To investigate the effect of the precise location of the second drop, we investigate the growth dynamics for different shifts, i.e. different initial positions. As an example a droplet with a contact angle of  $85^\circ$  is moved by the default distance of 2 lattice sites. The result is shown in figure 3, where the bridge height  $h_b$  in time  $t$  for different values of shift is recorded. As expected, overlapping droplets coalesce with an initial non-zero bridge height. By contrast, small separations between the drops cause a delay of the coalescence process by multiple timesteps. In this case diffusion occurs across the small separation of droplets, so that it takes some time before a detectable bridge has formed between the two drops. Further separation of the droplets causes the

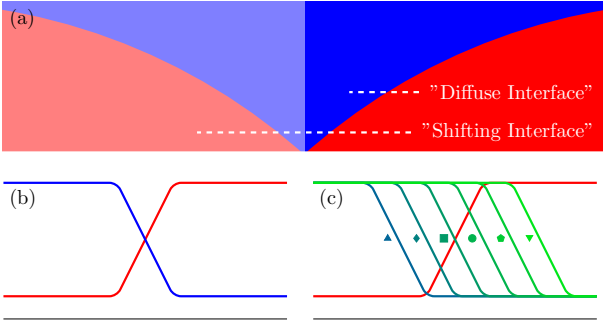


**Fig. 2** (Color online) (a) Schematic drawing of droplets on a substrate, before coalescence. The opaque half is mirrored through a free slip boundary. The density line cross section of Fig. (b) is indicated by the dashed line “Diffuse Interface” and the corresponding cross section of (c) is indicated with “Shifting Interfaces”. (b) Schematic of the density of red and blue fluid in a 1D cross section across the diffuse interface, as can be found along the dashed line “Diffuse Interface” in (a). The width of the diffuse interface is about six lattice sites. (c) The density cross section at the interface after moving the droplet to initialize coalescence. Only the density of the droplets is shown. Different possible options to shift the droplet are depicted by a left-right transition of the right droplet’s density field. The symbols correlate to those in Fig. 3.

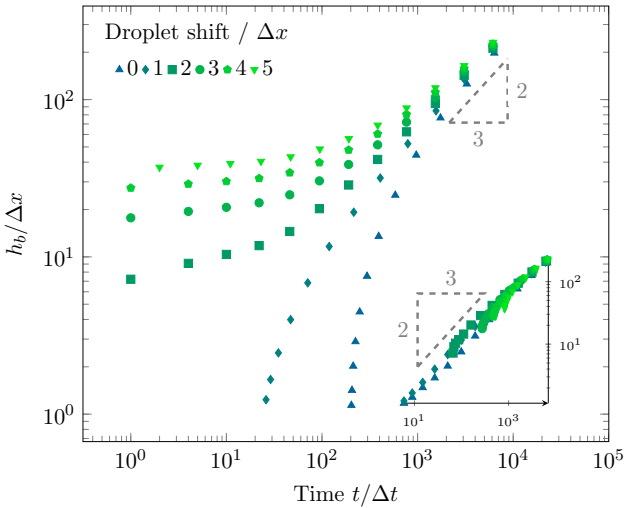


**Fig. 3** (Color online) The meniscus height in time of differently shifted droplets with a contact angle of  $85^\circ$ . This shift was implemented to trigger the coalescence after proper initialization of the diffuse interface. Overlapping droplets coalesce with an initial bridge height  $\geq 0$ . It can be seen that droplets with a small separation coalesce as well, but with a delay. Further separation of the droplets results in a system where the droplets do not coalesce for  $\geq 10000$  timesteps. It can be seen that the growth rate after initial coalescence, apart from minor initialization effects, is identical for different droplet shifts. The inset displays the same data, manually shifted. It can be seen that, apart from a small startup phase, these curves coincide. The initial timestep of coalescence is therefore highly dependent on two parameters: The choice of the density defined as the interface position and the initial shift.

coalescence not to occur for several thousand timesteps. After  $\approx 10^3$  timesteps all curves fall on a  $t^{2/3}$  power law. In the inset of Fig. 3 it is shown that a collapse of the data can be achieved by manual shift of the time, which is a robust way to identify an appropriate definition of  $t = 0$ . This procedure will be followed for all plots in the remainder of the paper.

### 3 Results

In Fig. 4 we show snapshots of the coalescence process at the exemplary contact angles of  $73^\circ$  and  $90^\circ$  (as is the case in the experiments of [40]). To represent the interface we use a bilinear interpolation of a threshold density which allows to obtain smooth data. The time series shows that a thin bridge appears between the two droplets, which grows both in height and width as time evolves. To quantify this evolution, we track the bridge height  $h_b(t)$  for a broad range of contact angles. This is shown in Fig. 5, where we show  $h_b$  (scaled with the drop radius  $r_0$ ) as a function of time (scaled with the inertio-capillarity time  $\sqrt{\rho r_0^3 / \gamma}$ ). The closed symbols represent simulations for various contact angles. For contact angles below  $90^\circ$ , the initial dynamics is consistent with a  $t^{2/3}$  power law until the bridge  $h_b$  becomes comparable to the drop size  $r_0$ . This is perfectly in line with experiments. When the contact angle is  $90^\circ$ , however, the slope of the data is smaller and suggests a smaller exponent, approaching the experimentally observed  $t^{1/2}$  scaling. For a more detailed comparison, we include in Fig. 5 the data from [40], which corresponds to experiments of water drops that coalesce in air. The experimental data shown here was shifted upwards, by a factor of 2, for the purpose of better visualization. However, even without this shift the experimental data lies about a factor 2 above the numerical data. This quantitative difference can possibly be attributed to the fact that the simulations consider droplets that are immersed into an outer fluid of equal density. The transport inside the outer fluid does slow down the dynamics with respect to the case of drops in air, which is consistent with the observations in Fig. 5. Therefore a quantitative match of these is not to be expected, but in terms of scaling laws the simulations comply with experiments. As the wettability of the substrate alters the contact angle of the fluid, it alters the capillary pressure of the droplets. Due to the capillary pressure driving the coalescence, the contact angle alters the rate at which the meniscus grows. The representative scaling laws for this behavior, as well as the behavior of the fluid interface are discussed below.

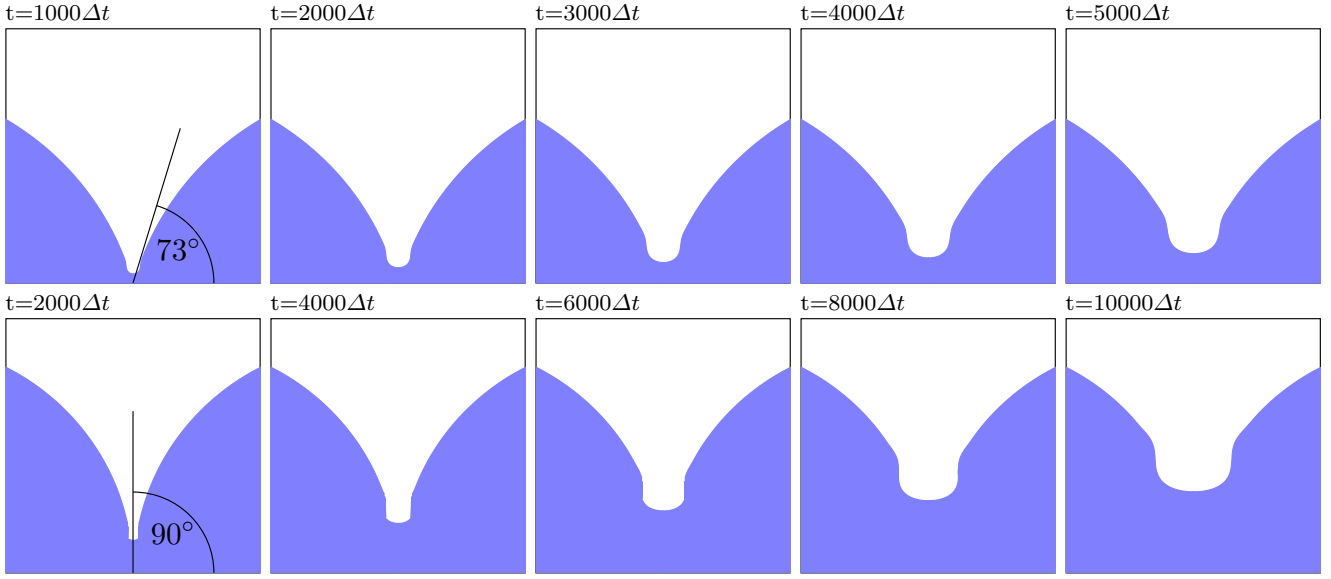


**Fig. 4** Time series of coalescence, zoomed into the meniscus shape. Upper row: Droplets with a contact angle of  $73^\circ$  at every 1000 timesteps. Lower row: Droplets with a contact angle of  $90^\circ$  at every 2000 timesteps. The number of timesteps are displayed above the snapshots.

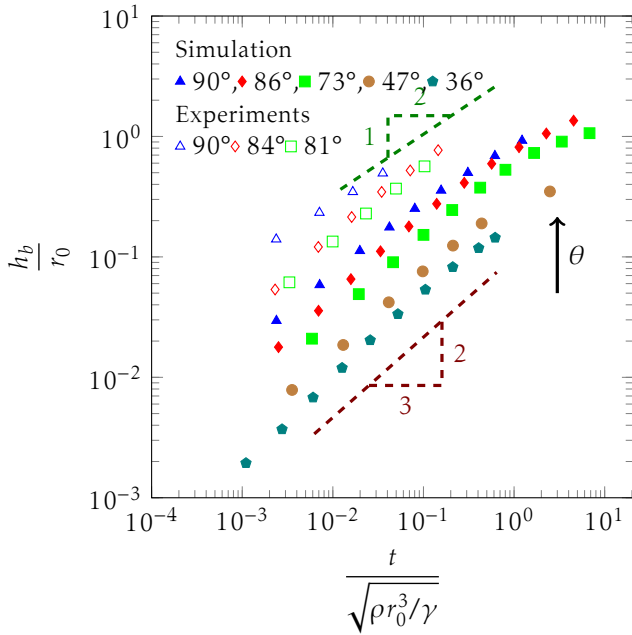


**Fig. 5** (Color online) The bridge height as a function of time for different contact angles  $\theta$ . The bridge height is scaled with the drop size, while time is rescaled by the inertio-capillary time. Closed symbols correspond to simulation results. Open symbols are experimental data for water drops in air, taken from [40]. For visual clarity, all experimental data has been multiplied with a factor of 2, to avert overlay.

### 3.1 Results for $\theta < 90^\circ$

To make further use of the simulation results, let us briefly revisit the usual scaling arguments for coalescence.

The situation is best understood for contact angles  $\theta < 90^\circ$ , for which the horizontal scale and vertical scale are simply proportional to one another: the ratio of the two lengths is set by the tangent of the contact angle. This can for example be seen from Fig. 4, showing that the width of the meniscus increases as well as  $h_b$  during the growth. Since  $h_b$  sets the characteristic scale of the bridge, the capillary pressure can be estimated as

$$P_{\text{cap}} \propto \frac{\gamma}{h_b}. \quad (4)$$

Similarly, the inertial pressure is obtained as

$$P_{\text{iner}} \propto \rho \left( \frac{h_b}{t} \right)^2, \quad (5)$$

which then leads to the observed

$$h_b \propto t^{\frac{2}{3}}. \quad (6)$$

To further test the idea that the dynamics is governed by the growing length scale  $h_b(t)$ , one can attempt a collapse of the bridge profiles during the growth process. This is shown for the case  $\theta = 73^\circ$  in Fig. 6, where we overlay the meniscus shapes for different times, after rescaling the horizontal and vertical scales with  $h_b(t)$ . The scaled profiles indeed exhibit an excellent collapse. This confirms that the bridge growth is characterized by a universal spatial profile, and that the temporal dependence can be effectively absorbed in the growing length scale  $h_b(t)$ . The self-similarity only applies for the initial stages of coalescence, so the data shown are until the bridge height reaches about one third of the initial drop height. This limits the data to parts of the

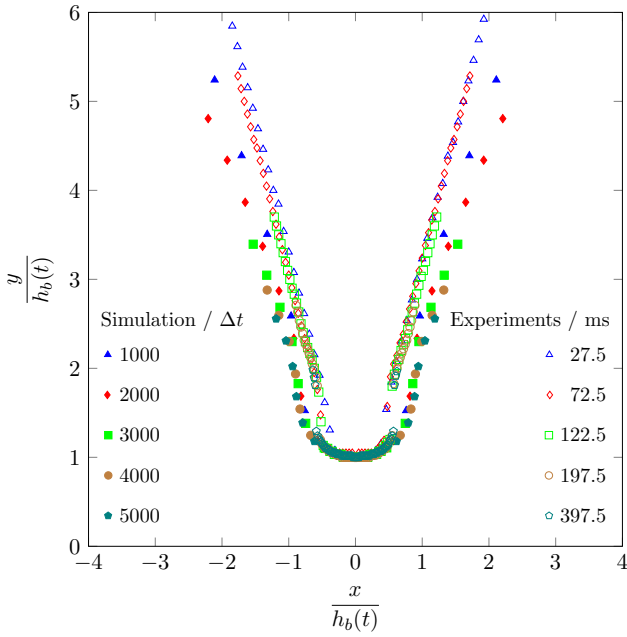


**Fig. 6** (Color online) Rescaled bridge shape for droplets with a contact angle of  $73^\circ$  reveal a self-similar bridge growth. Closed symbols correspond to simulation results, open symbols are experimental data for water drops in air [40].

droplet deformed by the coalescence, where the scaling law is applicable. Small deviations far from the meniscus can be attributed to this effect. Figure 6 also shows the corresponding experimental plot from [40], for which self-similarity was convincingly demonstrated as well. The numerical bridge shapes (for immersed drops) differ slightly from the experimental profiles, but the same principle of self-similarity is valid during the initial stages of coalescence.

Interestingly, the simulations allow one to extract information that is not easily accessible through experiments, such as the fluid velocities  $v_x$  and  $v_y$ . Inspired by the idea of self-similarity, we rescale the streamline patterns by again normalizing  $x$  and  $y$  by  $h_b(t)$ . The result is shown in Fig. 7, where the streamlines are obtained after scaling the velocities with  $h_b^{\frac{1}{2}}$  (different times are visualized using different colors). The streamline patterns exhibit an excellent collapse. It can be seen that the coalescence causes a recirculating flow, with a vortex located to the right of the symmetry axis, driving the meniscus upwards. The necessary rescaling of the velocity vectors can be understood by considering  $u \propto h_b/t \propto t^{-1/3}$ . This implies that  $uh_b^{1/2} = \text{const.}$ , as was indeed used in preparing Fig. 7.

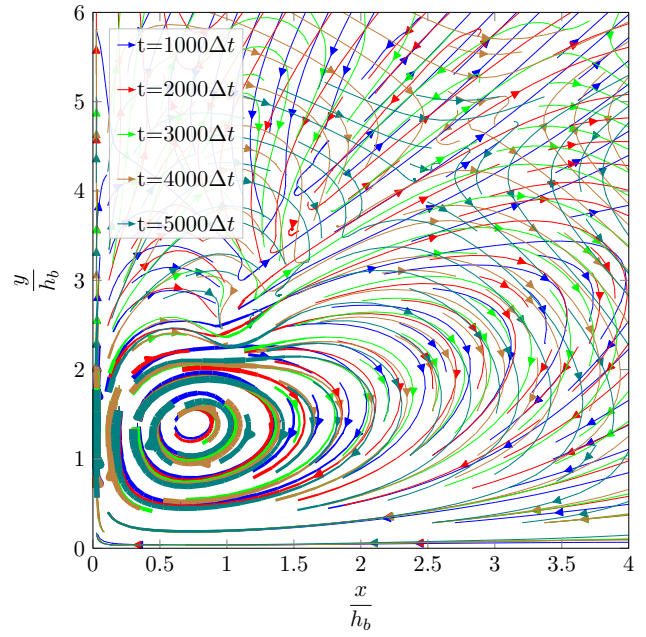


**Fig. 7** (Color online) Streamlines of the velocities in coalescing droplets with a contact angle of  $73^\circ$ , to the right of the symmetry axis. The positions of the velocities are rescaled like the interface positions. The amplitude of the velocities is scaled as  $v_x h_b^{\frac{1}{2}}$  and  $v_y h_b^{\frac{1}{2}}$ . The amplitude of the field is shown by varying the width of the streamlines linearly with the amplitude of the underlying vectors.

### 3.2 Results for $\theta = 90^\circ$

Let us now turn to the case of droplets with  $\theta = 90^\circ$ , for which the interfaces are tangent when brought into contact. As a consequence of this geometry, the horizontal and vertical scales are no longer the same. We therefore introduce the width of the bridge  $w$ , indicated in Fig. 1, as the horizontal scale that is much smaller than  $h_b$ . The geometry is such that

$$w \propto \frac{h_b^2}{r_0}, \quad (7)$$

and subsequently, the scaling laws need to account for this disparity of horizontal and vertical scales. The usual argument is that the capillary pressure reads

$$P_{\text{cap}} \propto \frac{\gamma}{w} \propto \frac{\gamma r_0}{h_b^2}, \quad (8)$$

which can be balanced with the inertial pressure

$$P_{\text{iner}} \propto \rho \left( \frac{h_b}{t} \right)^2. \quad (9)$$

This leads to

$$h_b \propto t^{\frac{1}{2}}, \quad (10)$$

and explains why the meniscus growth differs from the  $2/3$  law observed for smaller contact angles (cf. Fig. 5).



Once more, we will test these scaling ideas by searching for self-similar dynamics, both for the bridge shape and for the velocity profiles. The first of these tests is provided in Fig. 8, where the bridge profiles for  $\theta = 90^\circ$  are rescaled with  $w \sim h_b^2/r_0$  on the horizontal axis and with  $h_b$  in the vertical direction. A collapse is indeed observed, confirming the necessity of taking different horizontal and vertical scales. In addition the numerical profiles exhibit a perfect agreement with the experimental results for the bridge shape [40]. Intriguingly, however, we have not been able to obtain a convincing self-similarity for the velocity fields for  $\theta = 90^\circ$ . Following the logic above, one would expect for the horizontal velocity  $v_x \propto w/t \propto h_b^2/Rt \propto t^0$ , while for the vertical velocity  $v_y \propto h_b/t \propto t^{-1/2}$ . However, the best “collapse” was obtained by empirically scaling the velocities respectively as  $v_x h_b^{\frac{1}{3}}$  and  $v_y h_b^{\frac{1}{2}}$ , and the result is shown in Fig. 9. One again observes a recirculating flow that leads to the bridge growth, but the associated vortex structure is not perfectly self-similar. In particular, we note that the vortex appears to become smaller in time, after rescaling, suggesting that  $h_b$  and  $w$  are not the correct scales for the velocity field. The velocities of strongest amplitude lie underneath the meniscus and are nearly only vertical. Mass conservation in this case is achieved by enlarging the respective area in time. This means that the usual scaling arguments of equations 8 and 9 might actually be too simplistic. For example, the self-similar scaling of the meniscus profiles implies that the typical curvature scales as  $h_b/w^2 \sim r_0^2/h_b^3$ , and not as  $1/w \sim r_0/h_b^2$ , as was assumed in (8). This would change the coalescence exponent from  $1/2$  to  $2/5$ , which does not concur with simulations and previous experiments. This observation on the velocity field suggests that the pressure scaling (9) needs to be revised. The flow field is more intricate than the scaling argument allows to believe. Uncertainties in the definition of the scaling argument undermine this requirement. This would be an interesting topic for future work, for which a larger range of numerical data would be required to conclusively infer the relevant scaling laws. Droplets with a contact angle of  $90^\circ$  only differ from freely suspended coalescing droplets by a minor amount of surface friction. Therefore the scaling argument for freely floating droplets might need to be revisited as well.

#### 4 Conclusion

We simulated the coalescence of submerged droplets with different contact angles and compared our results to experimental data. Similar growth rates for the bridge height in time, equally dependent on the contact angle

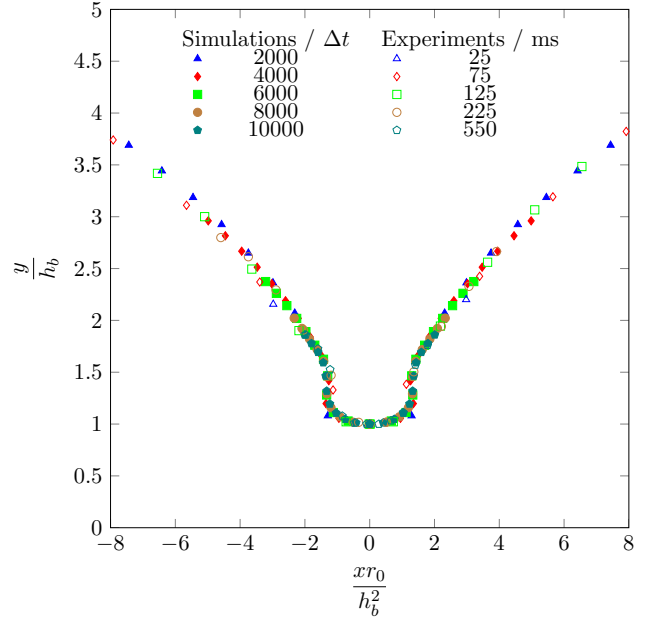


**Fig. 8** (Color online) Rescaled bridge shape for droplets with a contact angle of  $90^\circ$  reveal a self-similar bridge growth. Note that the horizontal and vertical axis are scaled differently. Closed symbols correspond to simulation results, open symbols are experimental data for water drops in air [40].

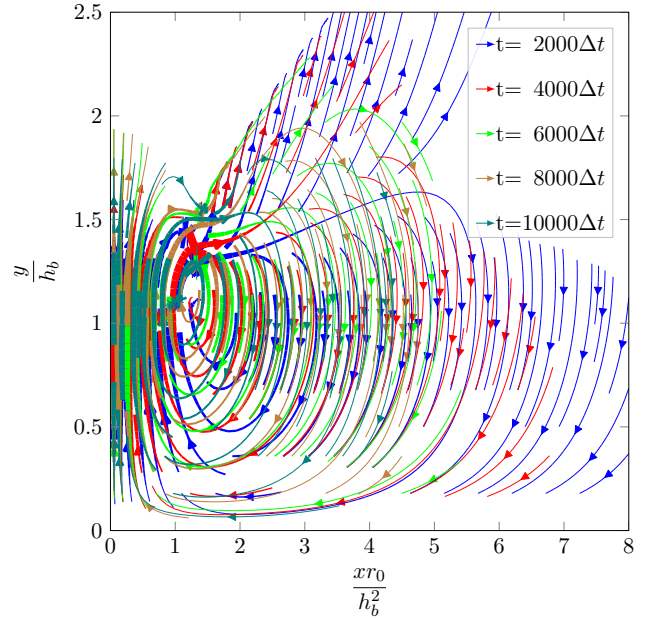


**Fig. 9** (Color online) Streamlines of the velocities in coalescing droplets with a contact angle of  $73^\circ$ , to the right of the symmetry axis. The positions of the velocities are rescaled like the interface positions. The amplitude of the velocities is scaled with the empirical values of  $v_x h_b^{\frac{1}{3}}$  and  $v_y h_b^{\frac{1}{2}}$ . The amplitude of the field is shown by varying the width of the streamlines linearly with the amplitude of the underlying vectors.

could be found in this case. Despite quantitative differences of the interface position of the fluid interface between experimental data of droplets in air and the simulation of submerged droplets, the same rescaling argument revealed a self similarity in time. Being able to use the same scaling arguments to scale the interface position of both the experimental droplets in air and the submerged simulated droplets shows the universality of the scaling argument. We applied this scaling law to the velocity field and, for droplets of a  $73^\circ$  contact angle, revealed the underlying velocities that cause the coalescence and give reasons for the scaling of the amplitude of the velocities. For droplets of a  $90^\circ$  contact angle we presented that the velocities causing the coalescence are more intricate than the scaling laws indicate. This shows that, though these scaling laws seem to work for the interface position, the underlying estimate for the relevant scaling for the velocity appears to be inconsistent with the internal flow structure. Clearly, our simulations show that the droplet internals are more complex than usually assumed. Our findings have implications for the design of devices in open microfluidics where different fluids are transported on chemically patterned substrates. Understanding the formation, transport and the coalescence of droplets in particular is mandatory to optimize these devices and ascertain a reliable long-term functionality.

## Acknowledgment

This research was carried out under project number M61.2.12454b in the framework of the Research Program of the Materials innovation institute M2i ([www.m2i.nl](http://www.m2i.nl)). We highly acknowledge Océ-Technologies B.V. for financial support and the Jülich Supercomputing Centre for the required computing time.

## References

1. F. Dörfler, M. Rauscher, J. Koplik, J. Harting, and S. Dietrich. Micro-and nanoscale fluid flow on chemical channels. *Soft Matter*, 8:9221–9234, 2012.
2. H. Gau, S. Herminghaus, P. Lenz, and R. Lipowsky. Liquid morphologies on structured surfaces: from microchannels to microchips. *Science*, 283:46–49, 1999.
3. S. Dietrich, M. Popescu, and M. Rauscher. Wetting on structured substrates. *Journal of Physics: Condensed Matter*, 17:S577, 2005.
4. A. A. Darhuber and S. M. Troian. Principles of microfluidic actuation by modulation of surface stresses. *Annu. Rev. Fluid Mech.*, 37:425–455, 2005.
5. M. Rauscher and S. Dietrich. Wetting phenomena in nanofluidics. *Annu. Rev. Mater. Res.*, 38:143–172, 2008.
6. J. W. van Honschoten, N. Brunets, and N. R. Tas. Capillarity at the nanoscale. *Chemical Society Reviews*, 39:1096–1114, 2010.
7. M. K. Chaudhury and G. M. Whitesides. How to make water run uphill. Technical report, HARVARD UNIV CAMBRIDGE MA DEPT OF CHEMISTRY, 1992.
8. F. Mugele and J.-C. Baret. Electrowetting: from basics to applications. *Journal of Physics: Condensed Matter*, 17:R705, 2005.
9. M. Rauscher, S. Dietrich, and J. Koplik. Shear flow pumping in open micro-and nanofluidic systems. *Physical review letters*, 98:224504, 2007.
10. A. van Tent and K. te Nijenhuis. The film formation of polymer particles in drying thin films of aqueous acrylic latices: II. Coalescence, studied with transmission spectrophotometry. *Journal of Colloid and Interface Science*, 232:350–363, 2000.
11. S. Karpitschka and H. Riegler. Sharp transition between coalescence and non-coalescence of sessile drops. *Journal of Fluid Mechanics*, 743, 2014.
12. M. Liu, J. Wang, M. He, L. Wang, F. Li, L. Jiang, and Y. Song. Inkjet printing controllable footprint lines by regulating the dynamic wettability of coalescing ink droplets. *ACS Applied Materials & Interfaces*, 6:13344–13348, 2014.
13. A. B. Thompson, C. R. Tipton, A. Juel, A. L. Hazel, and M. Dowling. Sequential deposition of overlapping droplets to form a liquid line. *Journal of Fluid Mechanics*, 761:261–281, 2014.
14. F. Liu, G. Ghigliotti, J. J. Feng, and C.-H. Chen. Numerical simulations of self-propelled jumping upon drop coalescence on non-wetting surfaces. *Journal of Fluid Mechanics*, 752:39–65, 2014.
15. S. Karpitschka, C. Hanske, A. Fery, and H. Riegler. Coalescence and noncoalescence of sessile drops: Impact of surface forces. *Langmuir*, 30:6826–6830, 2014.
16. J. Billingham and A. C. King. Surface-tension-driven flow outside a slender wedge with an application to the inviscid coalescence of drops. *Journal of Fluid Mechanics*, 533:193–221, 2005.
17. J. F. Hernández-Sánchez, L. A. Lubbers, A. Eddi, and J. H. Snoeijer. Symmetric and asymmetric coalescence of drops on a substrate. *Physical Review Letters*, 109:184502, 2012.
18. U. Sundararaj and C. W. Macosko. Drop breakup and coalescence in polymer blends: The effects of concentration and compatibilization. *Macromolecules*, 28:2647–2657, 1995.
19. M. Ahmadiouydarab and J. J. Feng. Motion and coalescence of sessile drops driven by substrate wetting gradient and external flow. *Journal of Fluid Mechanics*, 746:214–235, 2014.
20. Y. Sui, M. Maglio, P. D. M. Spelt, D. Legendre, and H. Ding. Inertial coalescence of droplets on a partially wetting substrate. *Physics of Fluids*, 25:101701, 2013.
21. M. Gross, I. Steinbach, D. Raabe, and F. Varnik. Viscous coalescence of droplets: A lattice Boltzmann study. *Physics of Fluids*, 25:052101, 2013.
22. D. Lohse and X. Zhang. Surface nanobubbles and nanodroplets. *Reviews of Modern Physics*, 87:981–1035, 2015.
23. H. J. C. Berendsen, J. P. M. Postma, W. F. van Gunsteren, A. DiNola, and J. R. Haak. Molecular dynamics with coupling to an external bath. *The Journal of Chemical Physics*, 81:3684–3690, 1984.
24. B. Bhushan, Y. Wang, and A. Maali. Coalescence and movement of nanobubbles studied with tapping mode AFM and tip-bubble interaction analysis. *Journal of Physics: Condensed Matter*, 20:485004, 2008.
25. B. M. Borkent, S. M. Dammer, H. Schönherr, G. J. Vancso, and D. Lohse. Superstability of surface nanobubbles. *Physical Review Letters*, 98:204502, 2007.



26. C. D. Bain and G. M. Whitesides. Formation of two-component surfaces by the spontaneous assembly of monolayers on gold from solutions containing mixtures of organic thiols. *Journal of the American Chemical Society*, 110:6560–6561, 1988.
27. J. T. Su and D. Needham. Mass transfer in the dissolution of a multicomponent liquid droplet in an immiscible liquid environment. *Langmuir*, 29:13339–13345, 2013.
28. P. B. Duncan and D. Needham. Microdroplet dissolution into a second-phase solvent using a micropipet technique: Test of the Epstein-Plesset model for an aniline-water system. *Langmuir*, 22:4190–4197, 2006.
29. D. Raabe. Overview of the lattice Boltzmann method for nano-and microscale fluid dynamics in materials science and engineering. *Modelling and Simulation in Materials Science and Engineering*, 12:R13, 2004.
30. S. Schmieschek and J. Harting. Contact angle determination in multicomponent lattice Boltzmann simulations. *Communications in Computational Physics*, 9:1165–1178, 2011.
31. J. D. Paulsen, J. C. Burton, and S. R. Nagel. Viscous to inertial crossover in liquid drop coalescence. *Physical Review Letters*, 106:114501, 2011.
32. J. D. Paulsen, J. C. Burton, S. R. Nagel, S. Appathurai, M. T. Harris, and O. A. Basaran. The inexorable resistance of inertia determines the initial regime of drop coalescence. *Proceedings of the National Academy of Sciences*, 109:6857–6861, 2012.
33. J. Eggers, J. R. Lister, and H. A. Stone. Coalescence of liquid drops. *Journal of Fluid Mechanics*, 401:293–310, 1999.
34. L. Duchemin, J. Eggers, and C. Josserand. Inviscid coalescence of drops. *Journal of Fluid Mechanics*, 487:167–178, 2003.
35. D. G. A. L. Aarts, H. N. W. Lekkerkerker, H. Guo, G. H. Wegdam, and D. Bonn. Hydrodynamics of droplet coalescence. *Physical Review Letters*, 95:164503, 2005.
36. J. E. Sprittles and Y. D. Shikhmurzaev. A parametric study of the coalescence of liquid drops in a viscous gas. *Journal of Fluid Mechanics*, 753:279–306, 2014.
37. W. D. Ristenpart, P. M. McCalla, R. V. Roy, and H. A. Stone. Coalescence of spreading droplets on a wettable substrate. *Physical Review Letters*, 97:064501, 2006.
38. R. D. Narhe, D. A. Beysens, and Y. Pomeau. Dynamic drying in the early-stage coalescence of droplets sitting on a plate. *EPL (Europhysics Letters)*, 81:46002, 2008.
39. M. W. Lee, D. K. Kang, S. S. Yoon, and A. L. Yarin. Coalescence of two drops on partially wettable substrates. *Langmuir*, 28:3791–3798, 2012.
40. A. Eddi, K. G. Winkels, and J. H. Snoeijer. Influence of droplet geometry on the coalescence of low viscosity drops. *Physical Review Letters*, 111:144502, 2013.
41. S. Mitra and S. K. Mitra. Symmetric drop coalescence on an under-liquid substrate. *Physical Review E*, 92:033013, 2015.
42. S. Succi. *The Lattice Boltzmann equation: For fluid dynamics and beyond*. Numerical Mathematics and Scientific Computation. Oxford University Press, Incorporated, 2001.
43. R. Benzi, S. Succi, and M. Vergassola. The lattice Boltzmann equation: Theory and applications. *Physics Reports*, 222:145–197, 1992.
44. S. Srivastava. *Lattice Boltzmann method for contact line dynamics*. PhD thesis, Eindhoven University of Technology, 2014.
45. Y.-H. Qian, S. Succi, and S. Orszag. Recent advances in lattice boltzmann computing. *Annu. Rev. Comput. Phys.*, 3:195–242, 1995.
46. X. Shan and H. Chen. Simulation of nonideal gases and liquid-gas phase transitions by the lattice Boltzmann equation. *Physical Review E*, 49:2941–2948, 1994.
47. H. Huang, D. T. Thorne, M. G. Schaap, and M. C. Sukop. Proposed approximation for contact angles in Shan-and-Chen-type multicomponent multiphase lattice Boltzmann models. *Physical Review E*, 76:066701, 2007.